PHILOSOPHICAL TRANSACTIONS OF THE ROYAL SOCIETY A MATHEMATICAL, PHYSICAL & ENGINEERING SCIENCES

Electrical Properties of Chain and Sheet Mercury Compounds

W. R. Datars, F. S. Razavi, R. J. Gillespie and P. Ummat

Phil. Trans. R. Soc. Lond. A 1985 **314**, 115-124
doi: 10.1098/rsta.1985.0012

Phil. Trans. R. Soc. Lond. A **314**, 115–124 (1985) [115]
Printed in Great Britain

Electrical properties of chain and sheet mercury compounds

By W. R. Datars, F. S. Razavi, R. J. Gillespie, F.R.S., and P. Ummat
McMaster University, Hamilton, Ontario L8S 4M1, Canada

The electrical resistivity of the chain compounds $Hg_{3-\delta}AsF_6$ and $Hg_{3-\delta}SbF_6$ decreases with decreasing temperature. It is shown that the temperature dependence of the resistivity of $Hg_{3-\delta}SbF_6$ depends on the rate that a sample is cooled from room temperature to liquid helium temperature. The electrical resistivity of the layered compounds Hg_3TaF_6 and Hg_3NbF_6 is metallic from 300 to 1.4 K. The induced torque, de Haas–van Alphen effect and resistivity of the chain compounds are related to the cylindrical Fermi surface model. Superconductivity of the compounds is discussed.

1. Introduction

Electrical conduction of chain and sheet mercury compounds results from conduction electrons of the mercury atoms and is of interest because of the unique structure of these compounds, which is expected to result in coupled one-dimensional or two-dimensional conduction. Previous electrical resistivity studies include work on $Hg_{3-\delta}AsF_6$ by Chiang *et al.* (1977), $Hg_{3-\delta}AsF_6$ and $Hg_{3-\delta}SbF_6$ by Cutforth *et al.* (1977) and $Hg_{3-\delta}AsF_6$ by Batalla & Datars (1982). Recent results of the temperature dependence of the resistivity of $Hg_{3-\delta}SbF_6$ are presented in §2. The temperature dependence of the resistivity of the sheet compounds is also given in that section. The electrical properties of the chain compounds are related in §3 to the Fermi surface determined by the de Haas–van Alphen effect (Razavi *et al.* 1979; Batalla *et al.* 1982). The superconductivity of the chain compounds is of interest because of results for $Hg_{3-\delta}AsF_6$ (Chiang *et al.* 1977; Spal *et al.* 1977; Batalla & Datars 1983; Schirber *et al.* 1982; Moses *et al.* 1983). The superconductivity of $Hg_{3-\delta}SbF_6$ is discussed in §4.

The chain mercury compounds consist of mercury in a tetragonal lattice of hexafluoride ions (Gillespie *et al.*, this symposium). The chains of mercury atoms are in channels in two mutually perpendicular directions. The mercury–mercury distance is incommensurate with the tetragonal host lattice. The chain compounds, which have a golden, metallic appearance, are $Hg_{3-\delta}AsF_6$, $Hg_{3-\delta}SbF_6$, $Hg_{3-\delta}TaF_6$ and $Hg_{3-\delta}NbF_6$. In contrast, the mercury in the sheet compounds is arranged on a hexagonal net in single sheets that are between layers of close-packed octahedral ions. The crystals are thin, flexible plates, which appear much different from the chain compounds.

2. Resistivity

Previous work shows that resistivities in the (001) plane of $Hg_{3-\delta}AsF_6$ and $Hg_{3-\delta}SbF_6$ are $10^{-4}\ \Omega$ cm and $1.1 \times 10^{-4}\ \Omega$ cm, respectively, at room temperature (Cutforth *et al.* 1977). The resistivities decrease with decreasing temperature down to liquid helium temperatures with a resistivity ratio between room temperature and 4.2 K of 500 for $Hg_{3-\delta}AsF_6$ and 300 for $Hg_{3-\delta}SbF_6$. Thus the chain compounds are metallic over this temperature range and there is

no evidence of a Peierls metal–insulator transition, which is predicted for a one-dimensional metal. This indicates that the chain compounds are not one-dimensional conductors and that perpendicular mercury chains are coupled.

Our results now indicate that the resistivity of $Hg_{3-\delta}SbF_6$ depends on how a sample is cooled from room temperature to 4.2 K. In samples that are cooled slowly over a period of one day, the resistivity follows the temperature dependence in figure 1. There is an inflection between 200 and 210 K, which is associated with the transition that is also observed in other experiments (Chartier *et al.* 1983). The temperature dependence is not linear at lower temperatures and can be fitted to a power law $T^{1.4}$ below 180 K. This is similar to that observed previously (Cutforth *et al.* 1977). However, this change of resistivity as a function of temperature is not observed after a sample is cooled quickly in 4 min from room temperature to 4.2 K. The resistivity measured as temperature is increasing is shown in figure 2. There is a large change of slope between 50 and 60 K. This indicates that different electron scattering processes exist at low and high temperatures in quickly cooled samples. The cooling rate does not affect electron scattering by the host lattice. However, it can affect short-range, parallel-chain ordering and the long-range, perpendicular-chain ordering measured by Heilmann *et al.* (1979). If this ordering is not complete in quickly cooled samples, there is electron scattering from the disorder, which has a certain temperature dependence. It is suggested that the disorder anneals between 50 and 60 K. The scattering from the ordered mercury chains then has a temperature dependence that is observed in the resistivity above 60 K.

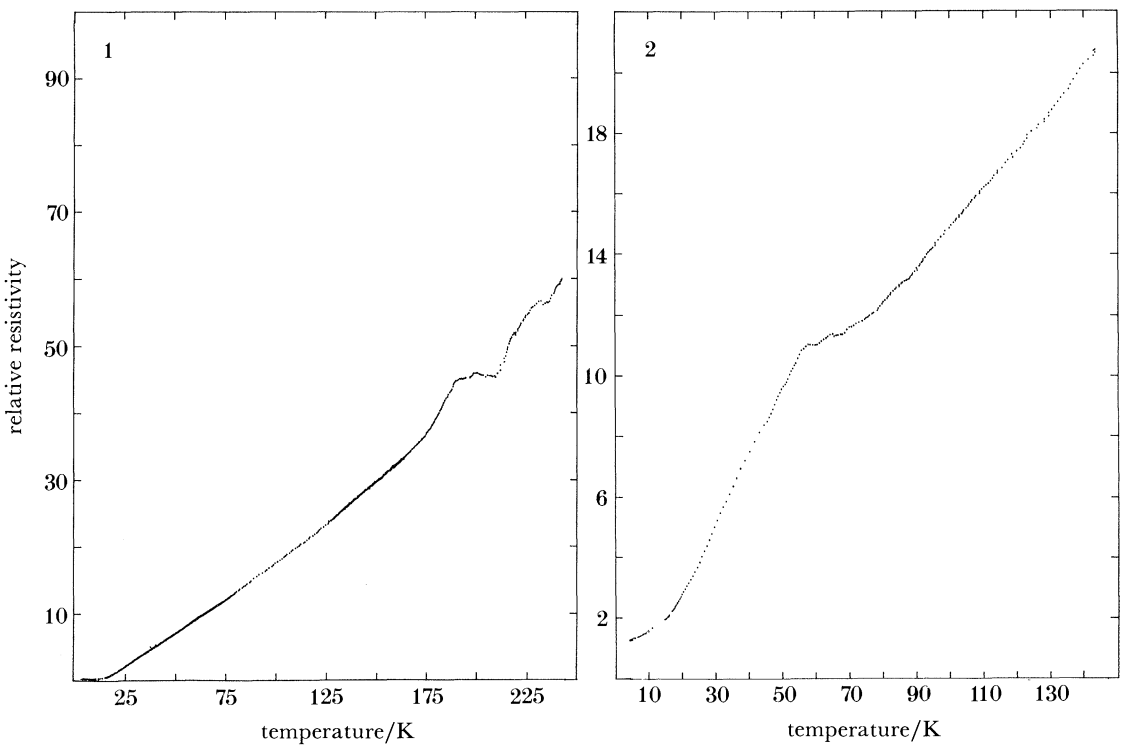

FIGURE 1. Electrical resistivity of a sample of $Hg_{3-\delta}SbF_6$ after a sample is cooled slowly from room temperature to 4.2 K. The relative resistivity is 100 at room temperature.

FIGURE 2. Electrical resistivity of $Hg_{3-\delta}SbF_6$ after a sample is cooled quickly to 4.2 K. Resistivity is measured while temperature is increasing and the relative resistivity is 100 at room temperature.

Resistivity measurements also show that the chain compounds are anisotropic. The resistivity anisotropy ratio ρ_c/ρ_{ab} where ρ_c and ρ_{ab} are the resistivities along the c axis and in the ab plane, respectively, is 105 for $Hg_{3-\delta}AsF_6$ at room temperature and has a small temperature dependence, shown in figure 3, down to 4.2 K. The resistivity ratio of $Hg_{3-\delta}SbF_6$ is 40.

The resistivities at room temperature of Hg_3TaF_6 and Hg_3NbF_6 are $1.6 \times 10^{-4}\ \Omega$ cm and $0.1 \times 10^{-4}\ \Omega$ cm, respectively. Resistivity as a function of temperature is the same for Hg_3NbF_6 and Hg_3TaF_6. Figures 4 and 5 show that the relation is approximately linear from room temperature down to 35 K, below which there is a higher power of temperature ($T^{2.3}$) until there is saturation below 14 K. This temperature dependence is similar to that of common

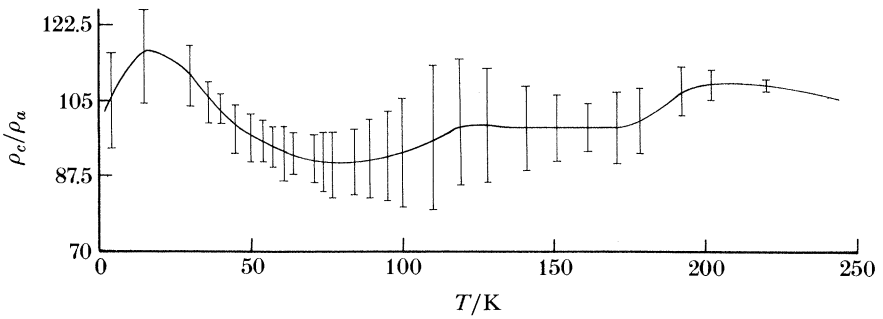

FIGURE 3. Experimental resistivity anisotropy as a function of temperature for $Hg_{3-\delta}AsF_6$. Error bars represent the variation in anisotropy from day to day while the continuous line follows the anisotropy over one day.

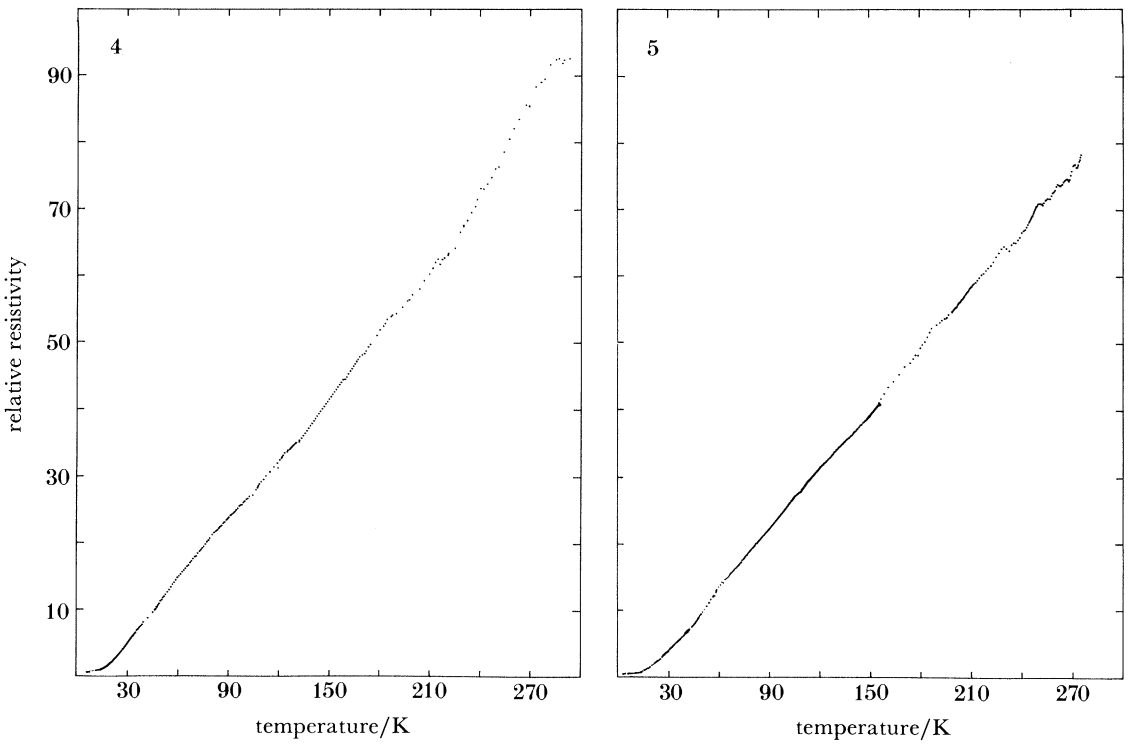

FIGURE 4. Relative resistivity of Hg_3NbF_6 between room temperature and 4.2 K. The relative resistivity is 100 at room temperature.

FIGURE 5. Relative resistivity of Hg_3TaF_6 between room temperature as 4.2 K. The relative resistivity is 100 at room temperature.

PHILOSOPHICAL TRANSACTIONS OF THE ROYAL SOCIETY A MATHEMATICAL, PHYSICAL & ENGINEERING SCIENCES

metals. However, it is considerably different from that of the chain compounds for which a linear temperature dependence is not observed. Also, the transition between 200 and 210 K is observed only in the chain compounds. The resistivity anisotropy of the sheet compounds has not been obtained because it has not been possible to measure ρ_c due to penetration of the soft plates by the probes.

3. Fermi surface of chain compounds

The electrical and optical properties of the chain compounds are anisotropic and metallic, which suggests that the conduction electrons are localized in the channels containing the mercury chains. In this model, there is ionic bonding between the positively charged mercury chains and the hexafluoride anions and metallic bonding between mercury atoms along a chain. The 6s electrons of the Hg atoms not required for the ionic bond participate in the metallic bond.

The Fermi level is calculated by assuming that electrons in the metallic bond move in a cylindrically symmetric uniform potential along the direction of the chains and that chains do not interact, which implies that the electron energy depends only on the component of the wavevector $\boldsymbol{k}$ along the chain. Electron states are filled up to the Fermi wavevector k_F according to the Pauli principle.

The number of electrons per unit cell in the metallic bond of one chain is

$$2(3-\delta)-1 = 5-2\delta, \tag{1}$$

since there are 2 valence electrons on $(3-\delta)$ atoms, from which one is used for the ionic bond. The density of states in one direction is $a/2\pi$ and the spin degeneracy is 2 so that the number of states between the Fermi wavevectors $-k_F$ and k_F is

$$2(a/2\pi)\, 2k_F = 2(a/\pi)\, k_F. \tag{2}$$

Equating (1) and (2) so that states are filled up to the Fermi wavevector gives

$$k_F = \pi/a(2.5-\delta). \tag{3}$$

The Fermi wavevector for one chain is independent of the components of $\boldsymbol{k}$ perpendicular to the chain. Thus, k_F defines planes in k-space at $+k_F$ and $-k_F$ for chains along the a direction. A similar set of planes exists for chains along the b direction. States between the planes are filled out to the zone boundary.

Both sets of planes in a unit cell are shown in figure 6*a*. Here, they are translated to the first zone for which

$$k_F = \pi/a(0.5-\delta). \tag{4}$$

These planes intersect at lines parallel to k_c where electron states in the two planes are degenerate. This degeneracy is removed, as illustrated in figure 6*b* by interaction between electrons on perpendicular chains. This forms an electron cylinder along k_c at the centre of the zone and hole cylinders with their axes along the corners of the zone. This defines the Fermi surface shown in the (001) plane in figure 6*c*.

Evidence for these cylinders is obtained by applying a magnetic field perpendicular to the c axis. Then electron states move along k_c and form open orbits. These open orbits cause an

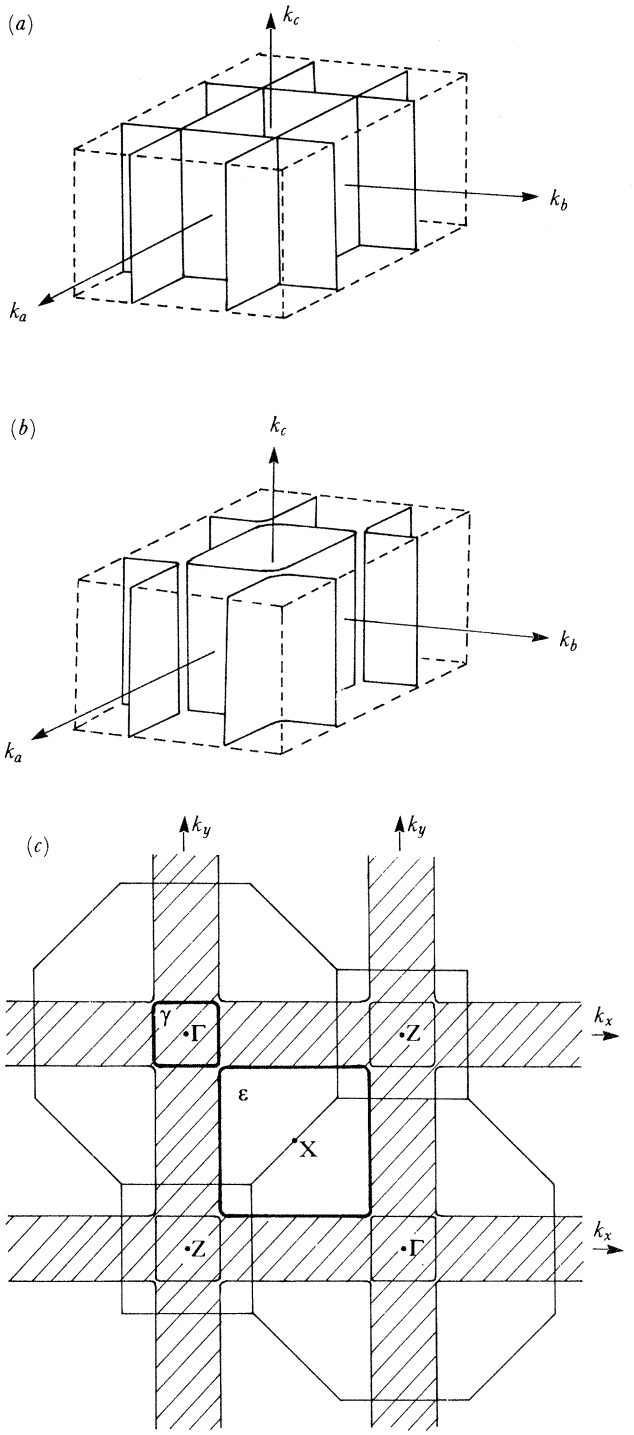

FIGURE 6. (*a*) Planes at $\pm k_F$ perpendicular to the k_a and k_b axes in the first zone of the chain compounds. (*b*) Removal of degeneracy at the intersection of the planes at the Fermi wavevector. (*c*) Cross section of the Fermi surface of $Hg_{3-\delta}AsF_6$ and the body-centred tetragonal Brillouin zone in the (001) plane in the extended zone scheme. Cross-hatched regions are occupied by electrons. The electron orbit γ and the hole orbit ε are outlined.

PHILOSOPHICAL TRANSACTIONS OF THE ROYAL SOCIETY A MATHEMATICAL, PHYSICAL & ENGINEERING SCIENCES

induced torque peak with the magnetic field perpendicular to the c direction, as shown for $Hg_{3-\delta}AsF_6$ at a magnetic field direction of 0° in figure 7. Small peaks in other directions in figure 7 are attributed to open orbits in [01n] directions with $n \geqslant 2$. They occur by magnetic breakdown of electrons across the energy gap separating the electron and hole cylinders. The well-defined directions of these open orbits shows that the magnetic breakdown occurs at only one point in the zone along k_c. This is the point of minimum separation. Thus, there is a variation of the separation of the cylinders along k_c. Such an undulation of the separation is obtained by Datars & Dinser (1984) by calculating electronic energy of overlapping wavefunctions in channels of the tetragonal lattice.

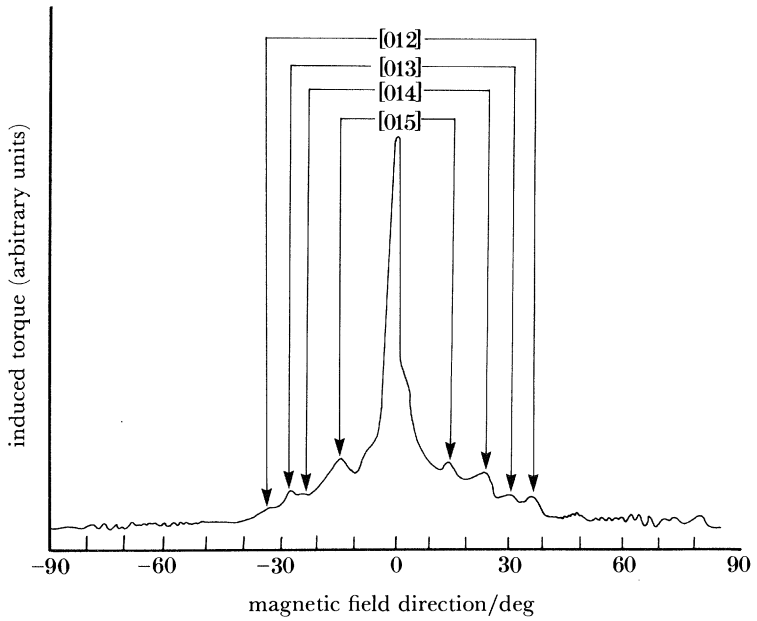

FIGURE 7. Induced torque as a function of magnetic field direction in a plane perpendicular to the (001) plane. The field is parallel to the (001) plane at 0°. The lines indicate calculated directions of open-orbit peaks.

The anisotropy of the resistivity gives additional insight into the Fermi surface. The electron velocity of an electron at a point defined by a wavevector $\boldsymbol{k}$ is always perpendicular to the Fermi surface at that point. Thus, the conductivity is maximum in the (001) plane and is zero along the direction for a plane Fermi surface. The non-zero conductivity along the c axis then implies that the Fermi surface is not plane and has an undulation along k_c with the periodicity of the lattice so that there is a component of electron velocity along the c axis. The deviation from a plane is estimated to be 2% of the Fermi energy for the observed anisotropy in the relative resistivity of 105 between 50 K and 300 K. The undulation is caused by interaction of the mercury chains.

Scattering processes of electrons on the Fermi surface are examined for a plane Fermi surface. Phonons from the three-dimensional host lattice and the one-dimensional mercury chains take part in the electron scattering as shown in figure 8. It should be noted first that scattering from $\boldsymbol{k}$ to $\boldsymbol{k}'$ on the same plane surface does not change the direction of velocity and does not cause resistance. However, scattering from one plane to a surface perpendicular to it gives rise to a resistivity labelled $\rho_\perp$. Scattering between plane surfaces at $+k_F$ and $-k_F$ gives rise to $\rho_\parallel$. Four

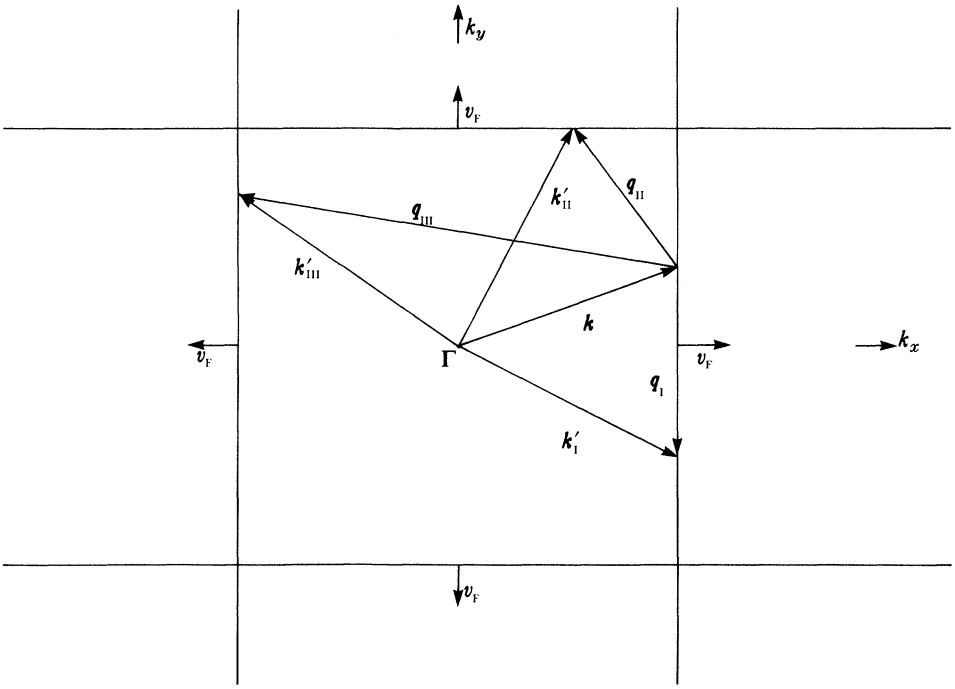

FIGURE 8. Electron–phonon scattering processes on the Fermi surface of mercury chain compounds. An electron in the kth state is scattered to $\boldsymbol{k}'_{\mathrm{I}}$, $\boldsymbol{k}'_{\mathrm{II}}$, $\boldsymbol{k}'_{\mathrm{III}}$, by phonons $\boldsymbol{q}_{\mathrm{I}}$, $\boldsymbol{q}_{\mathrm{II}}$, and $\boldsymbol{q}_{\mathrm{III}}$, respectively. The electron velocity $\boldsymbol{v}_{\mathrm{F}}$ is indicated on each Fermi surface.

terms in the resistivity for scattering by one-dimensional and three-dimensional phonons are therefore $\rho_{\perp}^{1\mathrm{D}}$, $\rho_{\perp}^{1\mathrm{D}}$, $\rho_{\parallel}^{3\mathrm{D}}$, and $\rho_{\parallel}^{3\mathrm{D}}$. The four resistivities are of the same order of magnitude above 15 K. Below 10 K, $\rho_{\perp}^{1\mathrm{D}}$ follows a T^2 temperature dependence while the other resistivities are decreasing more rapidly with decreasing temperatures. Therefore, the total resistivity is predicted to be proportional to T^2 below 2 K. Also, the peak in the anisotropy at low temperatures in figure 3 is due to the exponential decrease with decreasing temperature of three of the resistivities contributing to the resistivity in the (001) plane.

The cross section of the plane Fermi surface in the extended zone scheme in figure 6*c* shows the γ electron section and the ε hole section. The cross-sectional areas A are given by

$$A_{\mathrm{e}} = [\pi/a(1-2\delta)]^2, \tag{5}$$

$$A_{\mathrm{h}} = [\pi/a(1+2\delta)]^2, \tag{6}$$

for the electrons and holes, respectively. Measurement of these areas is made with the magnetic field along the c-axis from the frequency of the de Haas–van Alphen effect. There is excellent agreement between calculated and measured areas for both $Hg_{3-\delta}AsF_6$ and $Hg_{3-\delta}SbF_6$, as shown in table 1. Calculations are for $\delta = 0.21$ for $Hg_{3-\delta}SbF_6$ and $\delta = 0.135$ for $Hg_{3-\delta}SbF_6$. This agreement provides quantitative support for the Fermi surface model.

The two sets of chains order below 120 K and form two reciprocal lattices with common reciprocal points at

$$\boldsymbol{G} = n(3-\delta, \quad 3-\delta, 0). \tag{7}$$

These points are incommensurate with the reciprocal lattice of the anion lattice. Thus, translation of the plane Fermi surface by $\boldsymbol{G}$ is not coincident with the untranslated surface.

Table 1. Extremal cross-sectional areas perpendicular to the c axis of the Fermi surface of $Hg_{3-\delta}AsF_6$ and $Hg_{3-\delta}SbF_6$

orbit	(area for $Hg_{3-\delta}AsF_6$)/Å^{-2}		(area for $Hg_{3-\delta}SbF_6$)/Å^{-2}	
	experiment	theory	experiment	theory
α*	0.0046	0.0046	0.0330	0.0330
α	0.0325	0.0285	0.0735	0.0738
β	0.0395	—	—	—
γ	0.0598	0.0599	0.0931	0.0942
δ	0.178	0.178	0.160	0.161
μ	0.326	0.327	0.246	0.247
ε	0.325	0.359	0.258	0.259

This results in electron orbits α, α* and δ and hole orbits δ, ε and μ with areas shown in table 1, for $Hg_{3-\delta}AsF_6$ and $Hg_{3-\delta}SbF_6$. These orbits are detected in de Haas–van Alphen experiments and the measured areas of the orbits with the magnetic field parallel to the c axis in table 1 are in excellent agreement with theoretical areas.

4. Superconductivity

A superconducting transition was not observed in the resistivity of Hg_3TaF_6 and Hg_3NbF_6 although superconductivity in these sheet compounds was reported from susceptibility measurements (Datars *et al.* 1984). The transition observed in the susceptibility was therefore an experimental artifact and the superconductivity of the sheet compounds has not been established.

Superconducting properties of $Hg_{3-\delta}AsF_6$ have been investigated by a.c. susceptibility, magnetization and resistivity measurements.

A.c. susceptibility of a powder sample is shown as a function of magnetic field in figure 9 for the first and second times that the sample was cooled to liquid helium temperatures from

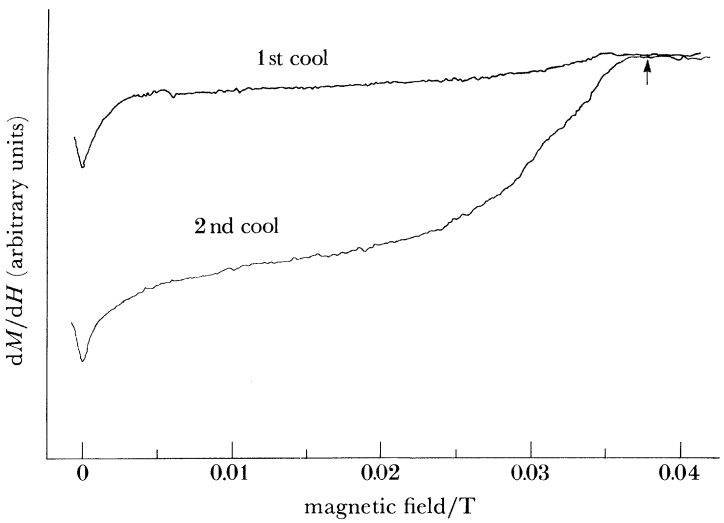

Figure 9. Magnetic susceptibility of a powder of $Hg_{3-\delta}AsF_6$ at 1.20 K as a function of magnetic field for the first and second time the sample is cooled from room temperature. The arrow indicates the critical field of mercury.

room temperature. The transition near 0.04 T is approximately six times larger after the second cool down while the minimum at zero field relative to the shoulder between 0.01 and 0.02 T remains the same size. So, there appear to be two distinct features in the susceptibility data, one near 0.40 T and one near zero field. The transition at higher fields is near the expected transition field of mercury shown by the arrow in figure 9.

The magnetic field of the high-field transition H_c plotted as a function of temperature in figure 10 is compared with a plot of

$$H_c/H_c(0) = 1-(T/T_c)^2. \tag{8}$$

Here, the critical field $H_c(0)$ at zero temperature and the critical temperature T_c at zero field are 0.0401 T and 4.14 K, respectively. These are very close to, but slightly less than the corresponding values for the rhombohedral α phase of metallic mercury of 0.0412 T and 4.152 K. It is not expected to be so in the mercury chains for which the coordination is much different than that of bulk mercury. Thus, the superconductivity near 4 K is attributed by Batalla & Datars (1982, 1983) to mercury dispersed throughout the sample. The mercury is probably in isolated, unconnected regions in the sample. However, it is not clear whether the mercury is in AsF_6^- vacancies or located elsewhere in the crystal.

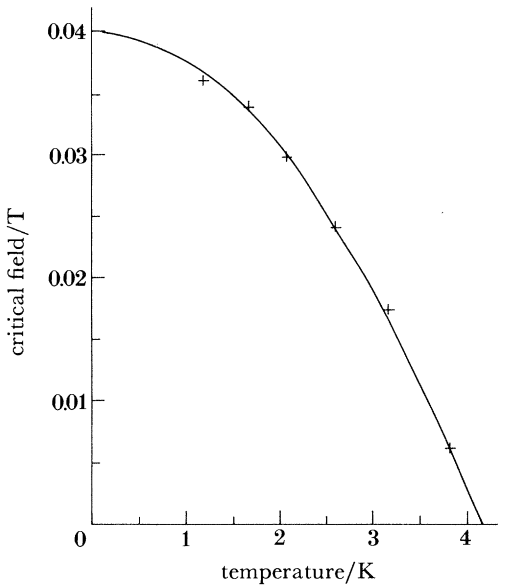

FIGURE 10. Critical field against temperature for the high-field transition of a powder of $Hg_{3-\delta}AsF_6$ fitted to equation (8).

The role of elemental mercury in the superconductivity of $Hg_{3-\delta}AsF_6$ has also been investigated by Schirber *et al.* (1982) by studying the pressure dependence of the transition. Elemental mercury undergoes a phase change with pressure from a simple rhombohedral α phase to a body-centred tetragonal β phase for which $T_c = 3.949$ K and $H_c(0) = 0.0339$ T. The critical field and temperature at zero pressure are close to those of α mercury in the experiment of Schirber *et al.* (1982). Application of pressure decreases the critical temperature of the compound by 0.2 K and changes the critical field to that of β mercury. The results strongly indicate that mercury dominates the superconductivity of $Hg_{3-\delta}AsF_6$ near 4 K.

However, the broadness of the transition at a temperature that is slightly below that of unconfined mercury indicates that the mercury is not completely free.

This mercury may be formed during cooling because the magnitude of the change at the transition depends on the number of times a sample is cooled to helium temperatures. Also, there is a melting exotherm in differential thermal analysis at the melting temperature of mercury (Datars *et al.* 1978; Chartier *et al.* 1983) which exists only after the sample is cooled below 195 K and indicates the presence of bulk mercury after cooling.

A transition in the resistivity along the *c* axis was observed near 4 K while the resistivity in the (001) plane was a continuous function of temperature (Chiang *et al.* 1977). This one-dimensional superconductivity was not found by Batalla & Datars (1983) in any sample with the resistivity measured in two ways. Thus, the one-dimensional superconductivity in resistivity is not reproducible, which would be possible if mercury is trapped in isolated regions that vary from sample to sample.

The superconducting properties of $Hg_{3-\delta}SbF_6$ are also interesting. Magnetic susceptibility measurements show a transition near 4.1 K with an amplitude that depends on the rate of cooling. There is also a change of susceptibility between 3 and 4 K. A transition that depends on the rate of cooling is also observed in the resistivity of $Hg_{3-\delta}SbF_6$ and does not depend on crystal orientation.

The research is supported by the Natural Sciences and Engineering Research Council of Canada.

References

Batalla, E. & Datars, W. R. 1982 *Can. J. Phys.* **60**, 1348–1357.
Batalla, E. & Datars, W. R. 1983 *Solid St. Commun.* **45**, 285–287.
Batalla, E., Razavi, F. S. & Datars, W. R. 1982 *Phys. Rev.* B **25**, 2109–2118.
Chartier, D., Datars, W. R. & Gillespie, R. J. 1983 *Can. J. Phys.* **61**, 71–75.
Chiang, C. K., Spal. R., Denenstein, A. M., Heeger, A. J., Miro, N. D. & MacDiarmid 1977 *Solid St. Commun.* **22**, 293–298.
Cutforth, B. D., Datars, W. R., van Schyndel, A. & Gillespie, R. J. 1977 *Solid St. Commun.* **21**, 377–379.
Datars, W. R. & Dinser, R. J. 1984 *J. Phys.* F **14**, 673–680.
Datars, W. R., Morgan, K. R. & Gillespie, R. J. 1983 *Phys. Rev.* B **28**, 5049–5052.
Datars, W. R., van Schyndel, A., Lass, J. S., Chartier, D. & Gillespie, R. J. 1978 *Phys. Rev. Lett.* **40**, 1184–1187.
Dinser, R. J., Datars, W. R., Chartier, D. & Gillespie, R. J. 1979 *Solid St. Commun.* **32**, 1041–1043.
Heilmann, I. U., Axe, J. D., Hastings, J. M., Shirane, G., Heeger, A. J. & MacDiarmid, A. G. 1979 *Phys. Rev.* B **20**, 751–762.
Moses, D., Denenstein, A. & Weger, M. 1983 *Phys. Rev.* B **28**, 6325–6328.
Razavi, F. S., Datars, W. R., Chartier, D. & Gillespie, R. J. 1979 *Phys. Rev. Lett.* **42**, 1182–1185.
Schirber, J. E., Heeger, A. J. & Nigery, P. J. 1982 *Phys. Rev.* B **26**, 6291–6293.
Spal, R., Chiang, C. K., Denenstein, A. M., Heeger, A. J., Miro, N. D. & MacDiarmid, A. G. 1977 *Phys. Rev. Lett.* **39**, 650–653.

PHILOSOPHICAL TRANSACTIONS OF THE ROYAL SOCIETY A MATHEMATICAL, PHYSICAL & ENGINEERING SCIENCES